Transport via nonlinear signal mixing in ratchet devices

Sergey E. Savel'ev, Fabio Marchesoni, Peter Hänggi, Franco Nori

Transport via nonlinear signal mixing in ratchet devices

Sergey Savel'ev,[1] Fabio Marchesoni,[1,2] Peter Hänggi,[3,1] and Franco Nori[1,4]

[1]*Frontier Research System, The Institute of Physical and Chemical Research (RIKEN), Wako-shi, Saitama, 351-0198, Japan*
[2]*Dipartimento di Fisica, Università di Camerino, I-62032 Camerino, Italy*
[3]*Institute of Physics, University of Augsburg, Universitätsstrasse 1, D-86135 Augsburg, Germany*
[4]*Center for Theoretical Physics, Department of Physics, University of Michigan, Ann Arbor, Michigan 48109-1120, USA*

The nonlinear signal mixing of two driving forces is used to control transport in *overdamped* ratchet devices. The interplay between the relative phase and the frequency ratio of the two driving forces is sufficient to generate an intriguing transport action that can be put to work to optimize shuttling and separation of particles in a variety of physical and technological applications. Analytic results for a striking multiple current reversal behavior including prominent, spikelike current features are obtained for doubly rocked and rocked-pulsated Brownian ratchets. This tunable signal mixing is readily implementable and exhibits even richer behaviors than those realized by the hard-to-implement modifiable-ratchet profiles.

PACS number(s): 05.40.−a, 05.60.Cd, 87.16.Uv

I. INTRODUCTION

Brownian ratchets or Brownian motors are nonlinear devices that, due to their intrinsic asymmetry, are capable of rectifying an external symmetric signal [1]. The simplest ratchet model is a Brownian particle diffusing in a periodic, asymmetric potential in one dimension. The input signal can be either deterministic (i.e., ac drive) or random and time correlated [2]. In particular, an ac signal can be injected so as to tilt periodically the ratchet potential (*rocked* ratchet [3]) or to modulate its amplitude with time (*pulsated* ratchet [4]). The fact that a random or deterministic signal is acting on the ratchet device means that the rectifying process occurs away from thermal equilibrium; being so, no conflict with the second law of thermodynamics occurs.

Here we study the case of a ratchet subjected simultaneously to two ac signals with periods $T_1 = 2\pi/\Omega_1$ and $T_2 = 2\pi/\Omega_2$. Our focus is on the case when Ω_1/Ω_2 is rational and does not address quasiperiodic drives [5]. We consider three distinct cases: (a) the two input signals are both additive and model a doubly rocked ratchet; (b) both signals are coupled multiplicatively to the ratchet potential, thus resulting in a doubly pulsated ratchet; (c) one ac signal drives the ratchet, while the other one multiplicatively modulates its amplitude (rocked-pulsated ratchet). We stress that experimental realizations of all cases are relatively straightforward to implement in the laboratory (mostly affordable variations of experimental setups widely reviewed in the literature [1]).

As an example of case (a) we mention transport of magnetic flux quanta (vortices) in superconducting devices [6–11], whereas some molecular motor experiments and quantum optical cold atom experiments [1] fall into categories (b) and (c). Asymmetric superconducting quantum interference devices (SQUIDS) [12,13] and Josephson junctions arrays [14] allow simple implementations of all the cases discussed here (i.e., doubly rocked, doubly pulsated, and rocked-pulsated ratchets), as such devices can be conveniently driven by independent external signals (either additive or multiplicative). Finally, a variety of tunable physical systems can be effectively controlled through the combined action of two (either independent or correlated) applied signals, like colloids in arrays of optical tweezers [15], interacting binary mixtures driven on (asymmetric) periodic substrates [16], ferrofluids [17], dislocation transport in crystalline solids [18,19], and electron pumping in quantum dots [20].

The key result of this work is that, no matter how we feed two periodic signals into a ratchet device, *signal mixing* determines a rich behavior of the ratchet dynamics depending on the input signal parameters (frequencies, phases, and amplitudes). In particular, we prove that the *rectification* of a primary signal by a ratchet *can be controlled more effectively by applying a secondary signal* (additive or multiplicative) with tunable frequency and phase than by tinkering with the ratchet potential parameters. The latter approach is inconvenient to implement experimentally, while modifying the input signals can be readily accomplished.

As in the overdamped, adiabatic regime the complication of chaos is absent, tuning the relative phase and the frequency ratio of the mixing drives provides a convenient and versatile way to inducing particle transport in a ratchet.

In Sec. II we introduce the simple model of a one-dimensional, overdamped ratchet device driven by two external input signals. Rectangular wave forms are adopted throughout in order to go beyond the well known *harmonic mixing* phenomenon [21–27] caused by the nonlinearity of the substrate rather than by its asymmetry. In Sec. III the case when both signals are coupled additively (doubly rocked ratchet) is studied under different adiabatic approximations. In Sec. IV we address the case of the two signals modulating the amplitude of the ratchet potential (doubly pulsated ratchet). In Sec. V A we consider the effects resulting from the combination of an additive and a multiplicative signal (rocked-pulsated ratchet). An example of the general case when signal mixing occurs due to the interplay of both asymmetry and nonlinearity is analyzed in Sec. V B. Specific physical examples for the application of these ideas are special SQUID devices, which are described in Sec. VI. The application of our approach to other systems (e.g., colloidal particles or vortices in superconductors) is straightforward.
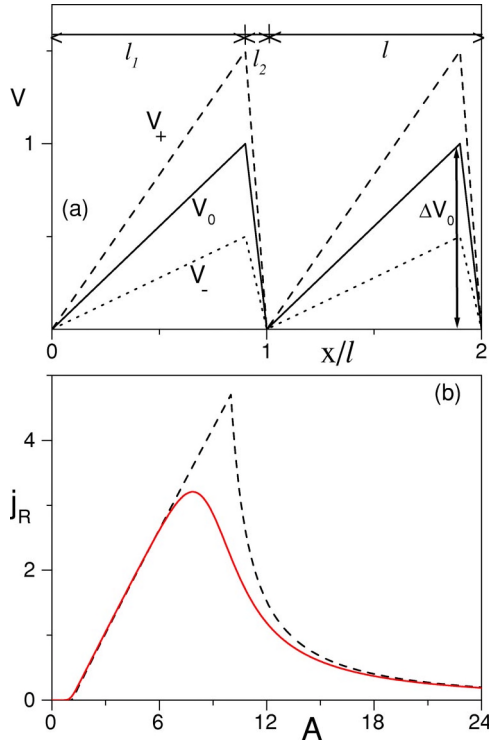
FIG. 1. (Color online) (a) Ratchet potentials. High V_+ and low V_- barrier configurations of the modulated potential $V(x,t)$, i.e., $V_\pm(x) = V_0(x)(1 \pm A_2)$ [$V_+(x)$, dashed curve above; $V_-(x)$, dotted curve below] with $A_2 = 0.5$. Reference ratchet potential (solid curve): $V_0(x) = qx/l_1$ for $0 < x < l_1$; $V_0(x) = q - q(x - l_1)/l_2$ for $l_1 < x < l = l_1 + l_2$, with $q = 1$, $l_1 = 0.9$, and $l = 1$. The barrier height ΔV_0 coincides with q. (b) Response curve $j_R(A)$ of the potential $V_0(x)$ driven by a rectangular force $A_1(t)$ with $A_1 = A$ ($A_2 = 0$) in the adiabatic limit $\Omega_1 \to 0$ at zero temperature, $D = 0$ (dashed, black curve), and low temperature, $D/\Delta V_0 = 0.05$ (solid, red curve).

In two Appendixes A and B we provide details of our analytical approach to the rectification mechanism in the adiabatic limit. Preliminary brief summaries of this work appeared in Ref. [28].

II. MODEL

Let us consider the simplest possible Brownian ratchet model: an overdamped Brownian particle $x(t)$ diffusing in a piecewise linear asymmetric potential $V_0(x)$ depicted in Fig. 1(a). Two rectangular input signals,

$$A_i(t) = A_i \, \text{sgn}[\cos(\Omega_i t + \phi_i)], \tag{1}$$

with $i = 1, 2$; $A_i \geq 0$ and $\text{sgn}[\cdots]$ denoting the sign of its argument $[\cdots]$, act on the particle according to the Langevin equation

$$\dot{x} = -V'(x,t) + A_a(t) + \xi(t), \tag{2}$$

where $\xi(t)$ is a stationary Gaussian white noise with $\langle \xi(t) \rangle = 0$ and $\langle \xi(t)\xi(0) \rangle = 2D\delta(t)$, and

$$V(x,t) = V_0(x)[1 + A_m(t)]. \tag{3}$$

Note that the noise strength D is proportional to the temperature, i.e., $D \propto T$.

Equation (2) allows these distinct ways of coupling an additional control signal $A_2(t)$ to a rocked ratchet driven by $A_1(t)$:

(a) doubly rocked ratchet,

$$A_m(t) = 0, \quad A_a(t) = A_1(t) + A_2(t), \tag{4}$$

(b) doubly pulsated ratchet,

$$A_a(t) = 0, \quad A_m(t) = A_1(t) + A_2(t), \tag{5}$$

with $A_1 + A_2 \leq 1$, and

(c) rocked-pulsated ratchet,

$$A_a(t) = A_1(t), \quad A_m(t) = A_2(t), \tag{6}$$

with $A_2 \leq 1$.

In our analytical discussion we assume that the intrawell (stochastic) relaxation takes place on a much shorter time scale than either both periods T_1 and T_2 (fully adiabatic), or one period, T_1 or T_2 (partially adiabatic). We also present results for the fully nonadiabatic case when both periods are comparable with the relaxation time. Without loss of generality, adopting the piecewise linear substrate potential $V_0(x)$

$$V_0(x) = \begin{cases} q \dfrac{x}{l_1} & \text{for } 0 < x < l_1, \\[2ex] q - q\left(\dfrac{x - l_1}{l_2}\right) & \text{for } l_1 < x < l = l_1 + l_2 \end{cases} \tag{7}$$

shown in Fig. 1(a) greatly simplifies the presentation below. The barrier height ΔV_0 coincides with q.

Our results have been obtained by using three different approaches:

(1) Direct simulation of the Langevin equation (2).

(2) Fully adiabatic treatment of the Fokker-Planck equation

$$\frac{\partial P}{\partial t} = \frac{\partial}{\partial x}\left\{ (V_0'[1 + A_m] - A_a)P + D\frac{\partial}{\partial x}P \right\}, \tag{8}$$

for the probability density $P(x,t)$ [1,3], by introducing the instantaneous probability current

$$j_{\text{dc}}(A_a(t), A_m(t)) = (V_0'[1 + A_m] - A_a)P + D\frac{\partial}{\partial x}P, \tag{9}$$

defined as its Stratonovich solution for A_a and A_m at time t. The average over the smallest common period $\tilde{T}$ for both applied signals is obtained by numerical integration:

$$j = \frac{1}{\tilde{T}}\int_0^{\tilde{T}} j_{\text{dc}}(A_a(t), A_m(t))\,dt. \tag{10}$$

(3) Analytical calculations developed for several special cases.
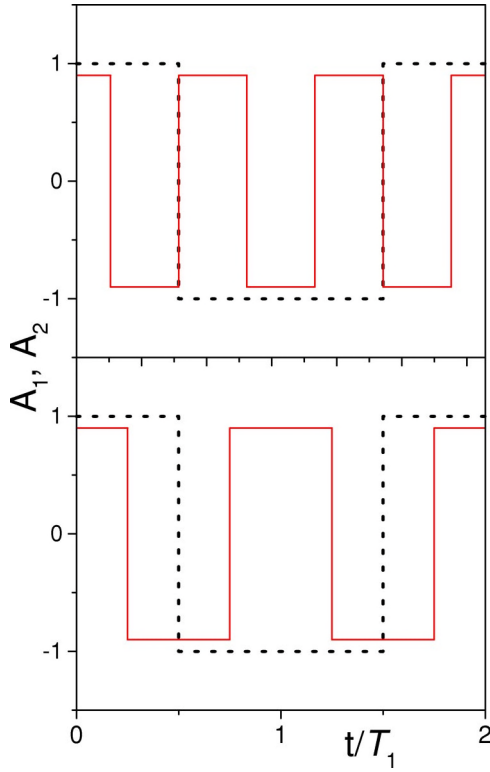
FIG. 2. (Color online) Input signals $A_1(t)$ (dashed) and $A_2(t)$ (solid) with $\Omega_2=3\Omega_1$ (upper) and $\Omega_2=2\Omega_1$ (lower); also $\phi_1=\phi_2=0$, $A_1=1$, and $A_2=0.9$.

III. DOUBLY ROCKED RATCHET

A. Fully adiabatic limit

The advantage of taking the *fully adiabatic* limit (Ω_1 and $\Omega_2 \to 0$) is that the output $j(\Omega_1,\Omega_2,A_1,A_2)$ of a doubly rocked ratchet is expressible analytically in terms of the current $j_R(A)$ of the well studied one-frequency rocked ratchet [3], corresponding to setting $A_1=A$, $A_2=0$ with $\Omega_1 \to 0$ [Fig. 1(b)]. Note that here $j_R(A)$ is a symmetric function of A,

$$j_R(A) = j_R(-A) = A[\mu(A) - \mu(-A)]/2, \qquad (11)$$

where $\mu(A)$ is the mobility of an overdamped particle running down the tilted ratchet potential $V_0(x)-Ax$. By inspecting Fig. 2, one concludes that the overall ratchet current $j(\Omega_1,\Omega_2,A_1,A_2)$ results from the interplay of the two usual one-frequency currents $j_R(A_1+A_2)$ and $j_R(A_1-A_2)$ driven by the ac amplitudes A_1+A_2 and A_1-A_2, respectively. That is, for driving with two odd numbered fractional harmonics, i.e.,

$$j\left(\Omega_1, \Omega_2=\Omega_1\frac{2m-1}{2n-1}, A_1, A_2\right)$$
$$= j_{\mathrm{av}}(A_1,A_2) - \frac{(-1)^{m+n}}{(2m-1)(2n-1)}\Delta j(A_1,A_2)p(\Delta_{n,m}),$$
$$(12)$$

with

$$\Delta_{n,m} = (2n-1)\phi_2 - (2m-1)\phi_1 \, \mathrm{mod}(2\pi), \qquad (13)$$

and

$$j_{\mathrm{av}}(A_1,A_2) = \frac{1}{2}[j_R(A_1-A_2) + j_R(A_1+A_2)], \qquad (14)$$

$$\Delta j(A_1,A_2) = \frac{1}{2}[j_R(A_1-A_2) - j_R(A_1+A_2)], \qquad (15)$$

for any integers m, n and $m>n$. The ϕ_1, ϕ_2 modulation is fully described by the multiplicative phase factor $p(\Delta_{n,m})$ with

$$p(\phi) = \frac{|\pi - \phi|}{\pi} - \frac{1}{2}. \qquad (16)$$

For non-odd fractional driving, i.e., $\Omega_2 \neq \Omega_1(2m-1)/(2n-1)$, the current equals the base value $j_{\mathrm{av}}(A_1,A_2)$.

Our analytical analysis yields the following results.

(1) The doubly rocked ratchet current (in the fully adiabatic limit) is insensitive to Ω_1,Ω_2 unless

$$\frac{\Omega_2}{\Omega_1} = \frac{2m-1}{2n-1}. \qquad (17)$$

Its intensity coincides with the "baseline" value $j_{\mathrm{av}}(A_1,A_2)$ of Eq. (14); spikes correspond to odd fractional harmonics; their amplitude $\Delta j(A_1,A_2)/(2m-1)(2n-1)$ is suppressed at higher harmonics, i.e., for larger m, n.

(2) The sign of the spike factor $\Delta j(A_1,A_2)$ is sensitive to the signal amplitudes A_1,A_2. For instance, if we choose A_1, A_2 so that A_1+A_2 and $|A_1-A_2|$ fall onto the rising (decaying) branch of $j_R(A)$ in Fig. 1(b), then $\Delta j(A_1,A_2)$ is negative (positive) (see Fig. 3).

(3) The current spikes at $\Omega_2/\Omega_1=(2m-1)/(2n-1)$ depend on the initial value of ϕ_1, and for a fixed ϕ_1, their amplitude oscillates with $\phi_2-\phi_1$ proportional to the modulation factor $p(\Delta_{n,m})$ (see Figs. 4 and 5).

All these properties are elucidated with Figs. 3–5, where results from numerical simulations are displayed. We remark that the overall sign of our doubly rocked ratchet is always determined by the polarity of $V_0(x)$ [positive in Fig. 1(a)], as $|\Delta j(A_1,A_2)| < |j_{\mathrm{av}}(A_1,A_2)|$ for any choice of A_1,A_2.

B. Partially adiabatic limit

In the *partially adiabatic* regime, where only one frequency tends to zero (say, $\Omega_1 \to 0$) multiple current inversions are possible (Fig. 6). The underlying mechanism hinges on the step structure of the one-frequency rocked ratchet current of particles traveling in a tilted potential $V_0 \mp |A_1|x$, for the nonadiabatic regime (see Fig. 7), where Ω_2 is still small but finite [3]. For instance, in the limit $\Omega_1 \to 0$ the net current of the doubly rocked ratchet (a) can be approximated to yield
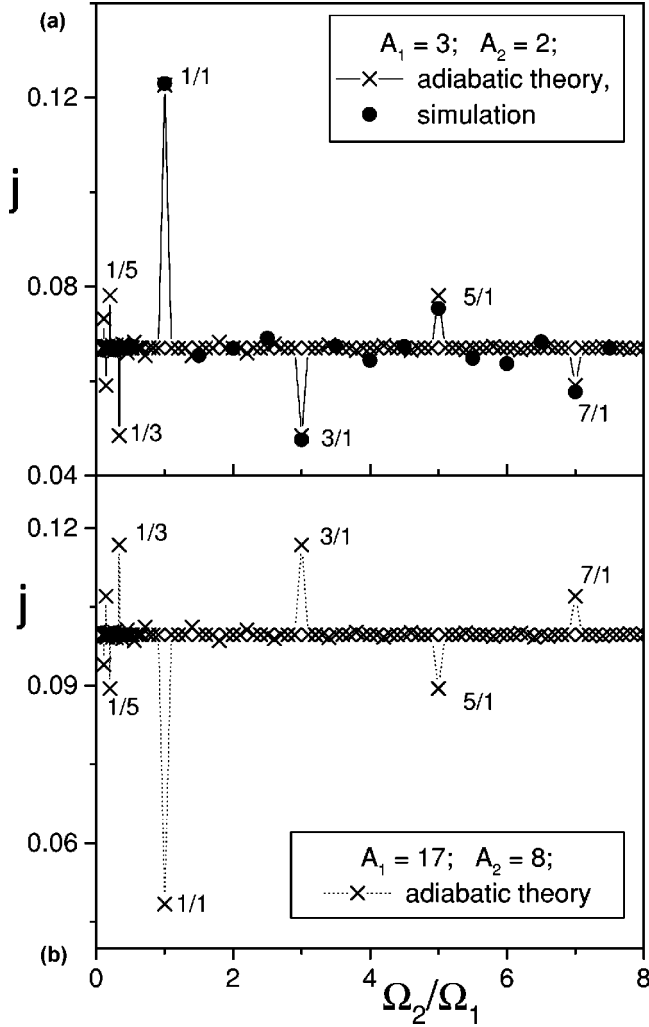
FIG. 3. Rectified current in a doubly rocked ratchet driven by two rectangular signals $A_1(t), A_2(t)$ and temperature, i.e., noise, $D = 0.6$. The substrate potential $V_0(x)$ is as in Fig. 1(a); see Eq. (7). $\Omega_1 = 0.01$ was kept constant and Ω_2 increased. (a) Numerical simulations for $\phi_1 = \phi_2 = \pi$ (circles) and fully adiabatic approximation (crosses). The amplitudes of the driving forces correspond to the rising branch of response curve j_R of Fig. 1(b), namely, $A_1 = 3$ and $A_2 = 2$. (b) The same as in (a) but for two amplitudes $A_1 = 17$ and $A_2 = 8$, belonging to the decreasing branch of j_R. In agreement with Eqs. (12)–(15), the current spikes in (a) and (b) are inverted. Ω_2/Ω_1 for most commensuration spikes is indicated explicitly by using $m/n (= \Omega_2/\Omega_1)$; spikes with larger m, n are hardly visible.

$$j(\Omega_1 \ll \Omega_2, A_1, A_2) = \frac{1}{2}[j_+(\Omega_2, A_2) + j_-(\Omega_2, A_2)], \quad (18)$$

where $j_\pm(\Omega_2, A_2)$ is the average current across the static tilted ratchet potential $V_0(x) \mp |A_1|x$ driven by the rectangular signal $A_2(t)$. Note that for $\Omega_2 \gg \Omega_1$ the commensuration spikes (12) can be neglected as they decay proportionally to Ω_1/Ω_2.

In order to clarify the resulting current structure (18), in Fig. 6 we consider the simplified case $A_1 = A_2 \equiv A$ and $\Omega_2 \gg \Omega_1$. During one half of the longer period $T_1/2$, the total ac force $A_a(t)$ switches many times either between 0 and $2A$ or between 0 and $-2A$ with frequency Ω_2. We also assume that
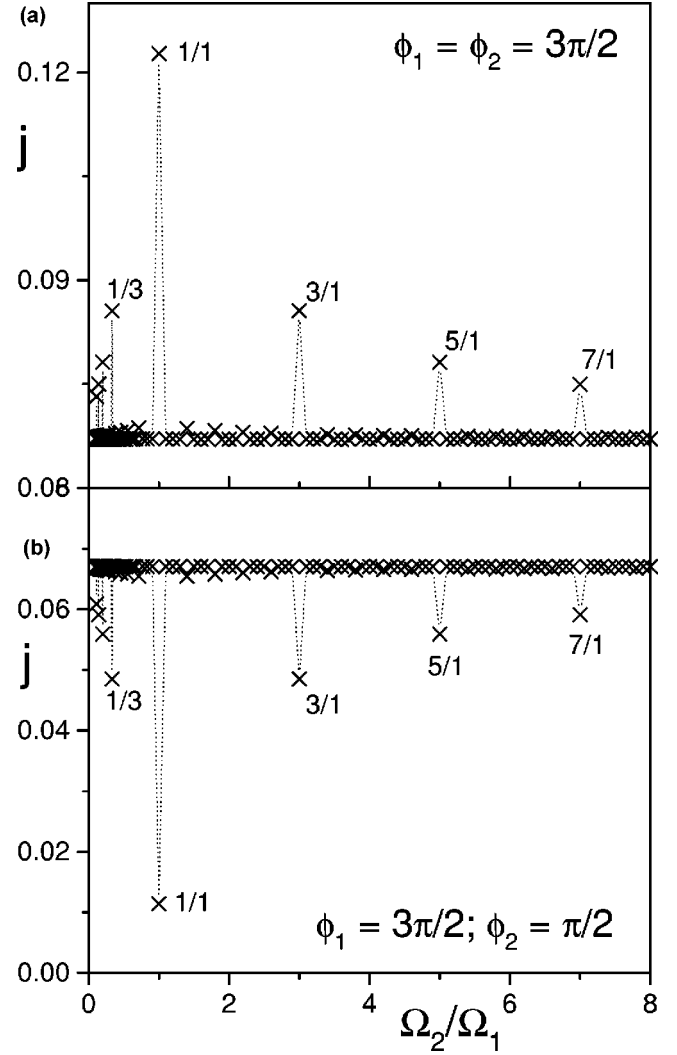
FIG. 4. Rectified current in a doubly rocked ratchet and driven by two rectangular signals $A_1(t)$ and $A_2(t)$ with fixed amplitudes $A_1 = 3$, $A_2 = 2$, and noise $D = 0.6$. The substrate potential $V_0(x)$ is as in Fig. 1(a); see Eq. (7). Calculations in the fully adiabatic approximation for $\phi_1 = \phi_2 = 3\pi/2$ (a) and $\phi_1 = 3\pi/2$, $\phi_2 = \pi/2$ (b). $\Omega_1 = 0.01$ was kept constant and Ω_2 increased. Due to phase modulation [see the factor $p(\Delta_{n,m})$ in Eqs. (12) and (16)], the current spikes in (a) and (b) are inverted; (m, n) spikes with larger m, n are hardly visible.

the higher forcing frequency Ω_2 is lower than the deterministic relaxation rate (cf. Fig. 1)

$$\Omega_q = \frac{\pi q}{l_1^2}, \quad (19)$$

i.e., the Brownian particle reaches a $V_0(x)$ minimum during each half period $T_2/2$ when $A_a(t) = 0$. As a consequence, the particle moves an integer number of unit cells l during each short period T_2, thus determining the steplike structure of the currents $j_\pm$ displayed in Fig. 7. A straightforward analytical calculation of the average particle velocity at zero noise level toward the right (left) yields (see Appendix A for details)
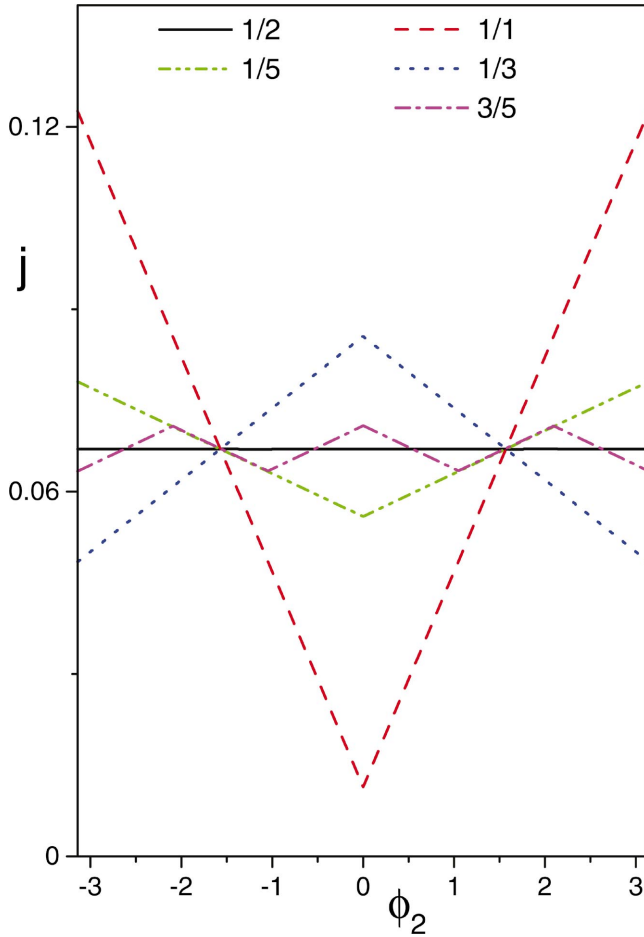
FIG. 5. (Color) Computed ratchet current j versus ϕ_2 in the fully adiabatic limit for $\phi_1=0$ and different values of Ω_2/Ω_1 (Ω_2/Ω_1 =1/1,1/2,1/3,1/5,3/5). Note the good agreement with the modulation factor $p(\Delta_{n,m})$ in Eqs. (12) and (16). Other simulation parameters are as in Fig. 4.

$$v_\pm(A) = \pm \frac{nl}{T_2} \qquad (20)$$

for

$$A_\pm^{(n+1)} < A < A_\pm^{(n)} \qquad (21)$$

and

$$v_\pm(A) = 0, \text{ for } A < A_\pm^{(1)}, \qquad (22)$$

with

$$A_\pm^{(n)} = \frac{1}{2} \left\{ \frac{(2n-1)l \pm \delta l}{2T_2} \mp f_{\text{net}} \right.$$
$$\left. + \sqrt{\left\{ \frac{(2n-1)l \pm \delta l}{2T_2} \pm f_{\text{net}} \right\}^2 + \frac{q^2}{l_1 l_2} + \frac{2q}{T_2}} \right\}, \quad (23)$$

$f_{\text{net}}=q\,\delta l/(2l_1l_2)$, and $\delta l=l_1-l_2$ (cf. Fig. 1), and where q denotes the barrier height of the ratchet potential. The analytical expression $[v_+(A)+v_-(A)]/2$ for the ratchet current compares very well with the simulation data displayed in Fig. 6.

We notice that on increasing A the resulting ratchet current develops a negative tail made of entrained rectangular teeth of the same size. Such a negative tail of noise-broadened teeth persists in the presence of noise, although the teeth become gradually suppressed, thus implying, at variance with the fully adiabatic limit, a robust inverted output signal.

Finally, for $A_2/A_1<1$ the particle current j depends on the driving amplitude in a much more complicated manner, though still expressible in terms of Eq. (18). For a small relative difference of ac amplitudes, $A_1-A_2\ll A_1$, the current $j(A)$ exhibits multiple current inversions, as seen in Fig. 8. At small amplitudes the curve j versus A is similar to that of Fig. 6 for $A_1=A_2=A$. At higher amplitudes, the current peaks change their shape from rectangular to triangular and the "running average" of $j(A)$, $\langle j \rangle_A$, taken over several peaks, increases steadily [Fig. 8(a), insets]. Noise smooths out the sharp peaks of $j(A)$ in Fig. 8(b). In other words, instead of having an average negative tail, the curve $\langle j \rangle_A$ turns positive above a certain value of A and then attains a positive maximum. For larger differences $(A_1-A_2)/A_1$, no current inversion occurs, as shown in Fig. 9; $j(A)$ exhibits two maxima for large enough noise (red dashed line in Fig. 9), corresponding to the superposition of two ratchet currents j_R [Fig. 1(b)] with shifted maxima.

C. Nonadiabatic regime

In a fully nonadiabatic regime the dependence of the particle current on the driving amplitude becomes more complicated. For instance, *multiple current inversions* have been detected with increasing amplitude A of the driving force

$$A_a(t) = A(\text{sgn}[\cos \Omega_1 t] + \text{sgn}[\cos \Omega_2 t]); \qquad (24)$$

see Fig. 10. Interestingly, even though j versus A is strongly suppressed for $\Omega_1=\Omega_2$ [see solid (red) curve in Fig. 10(a)], an appreciable ratchet effect persists when Ω_2 is increased beyond Ω_1 [see Figs. 10(b) and 10(c)]. This implies that a sustained *rectification* effect can be achieved in ratchet devices operating at high frequencies; namely, gradually increasing the frequency difference $\Omega_2-\Omega_1$ results first in current steps equal to $(\Omega_2-\Omega_1)l$ [Figs. 10(b) and 10(c)]; then the current steps become smaller and current spikes with different signs appear [Fig. 10(d)]; finally, in the limit $\Omega_2 \rightarrow \infty$, $j(A,\Omega_1,\Omega_2)$ evolves toward the value $j(A/2,\Omega_1,\Omega_1)$.

IV. DOUBLY PULSATED RATCHET

Here the Brownian particle diffuses in a pulsated potential $V(x,t)$, whose amplitude switches among four different values $\Delta V_0(1-A_1-A_2)$, $\Delta V_0(1+A_1-A_2)$, $\Delta V_0(1-A_1+A_2)$, and $\Delta V_0(1+A_1+A_2)$. As $m>n$, let us consider the two time-dependent potentials $V_0(x)[1-A_1+A_2(t)]$ for the half cycle $A_1(t)=-A_1$, and $V_0(x)[1+A_1+A_2(t)]$ for the remaining half cycle $A_1(t)=A_1$: They are both pulsated at the higher frequency Ω_2 and, therefore, sustain currents $j_{p1}(A_2)$ and $j_{p2}(A_2)$, respectively (proportional to Ω_2^2 for $\Omega_1\rightarrow 0$, e.g., [1]). Following the approach outlined in the previous case (a), and guided by the plots of $A_1(t)$, $A_2(t)$ in Fig. 2, one
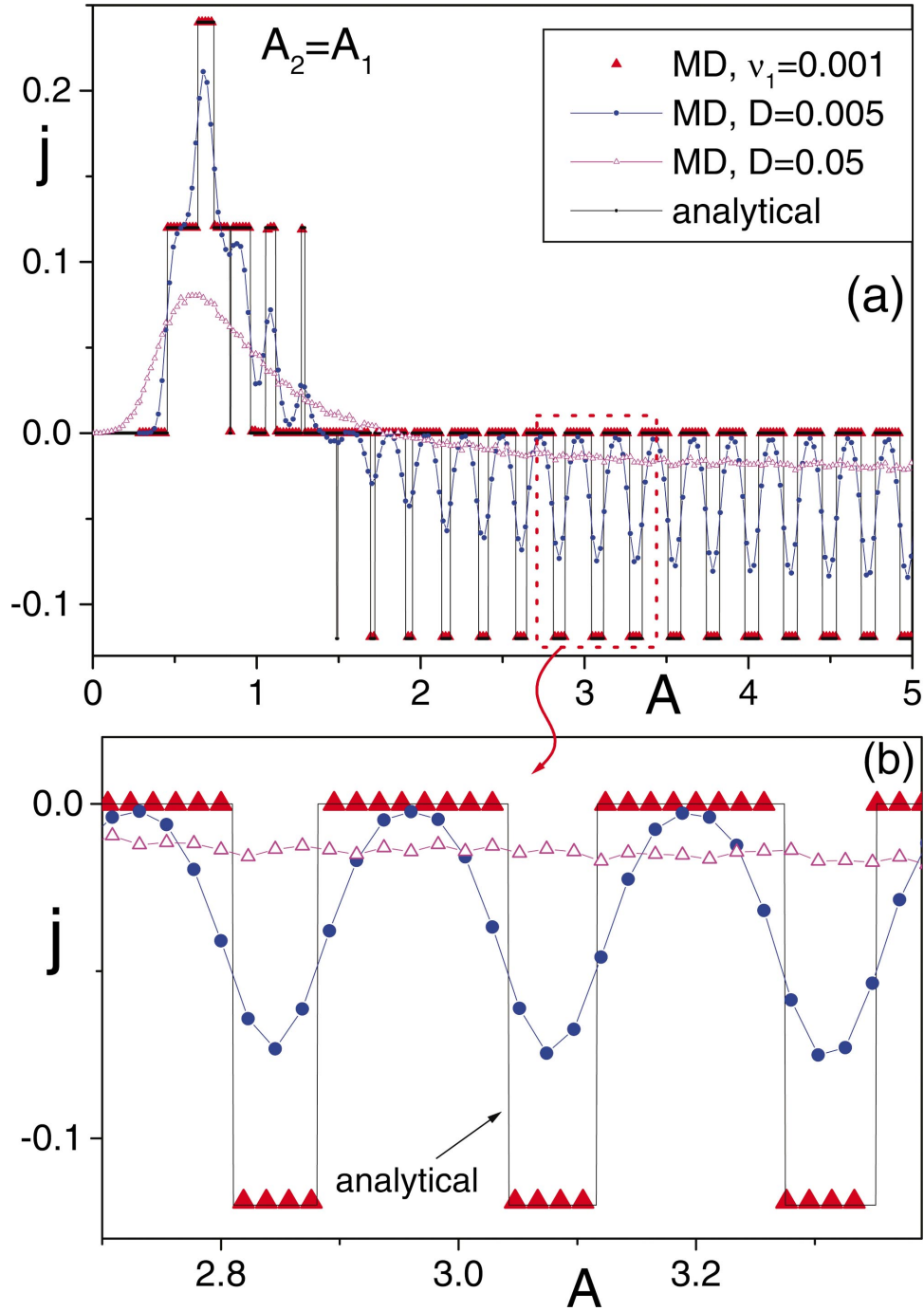
FIG. 6. (Color) Rectified current in the doubly rocked ratchet with $A_1=A_2=A$, $T_1=10^3$, $T_1/T_2=240$. (a) Simulation data for $D=0$ (red solid triangles), 5×10^{-3} (blue dots), and 0.05 (pink open triangles). The black solid curve with steps is our analytical prediction for $D=0$ (see text). (b) Blowup of the dashed, red box in (a). The ratchet potential $V_0(x)$ parameters are $q=0.4$, $l_1=0.7$, and $l=1$.

concludes that Eq. (12) applies to the present case, too, after replacing the definition (14) with

$$j_{av}(A_1,A_2) = \frac{1}{2}[j_{p1}(A_2) + j_{p2}(A_2)]. \qquad (25)$$

Note in this context that the sign of j_{av} becomes reversed here with respect to case (a). For

$$\Omega_2 = (2m-1)\Omega_1 \qquad (26)$$

one immediately recognizes the existence of an "odd harmonics" structure in the spectrum of the ratchet current, but, at variance with Eq. (12), no obvious factorization between the A_1,A_2 dependence and m,ϕ_2 modulation could be derived, as the adiabatic approximation is no longer tenable here. Nevertheless, even in this case, the spike amplitudes are still inversely proportional to the ratio Ω_2/Ω_1. Numerical
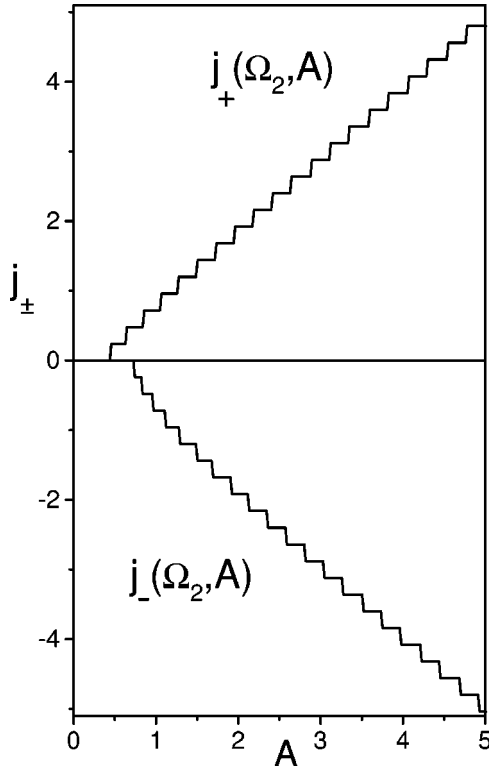
FIG. 7. Simulated net currents $j_\pm(\Omega_2, A_2)$ in the tilted rocked ratchet $V_0(x) \mp |A_1|x$ for $A_1 = A_2 \equiv A$, $\Omega_2 = 1.5$, and $D=0$; $V_0(x)$ parameters: $q=0.4$, $l_1 = 0.7$, and $l=1$. The current step structure is due to the fact that a particle moves sidewise an integer number of potential cells; hence the "quantization" of the relevant average velocities in units of $l\Omega_2$.

simulations support these predictions, as confirmed in Fig. 11.

V. ROCKED-PULSATED RATCHET

A. Mixing of two square-wave signals

The mixing of an additive and a multiplicative signal provides a *control mechanism* of potential interest in device design. In the *fully adiabatic* limit, the ac driven Brownian particle can be depicted as moving back and forth over two alternating ratchet potentials

$$V_\pm(x) = V_0(x)(1 \pm A_2). \qquad (27)$$

Both potential configurations $V_\pm(x)$ are capable of rectifying the additive driving signal $A_1(t)$; the relevant net currents $\overline{j}_\pm(A_1)$ are related to the curve $j_R(A)$ plotted in Fig. 1(b):

$$\overline{j}_\pm(A_1) = (1 \pm A_2) j_R\left[\frac{A_1}{1 \pm A_2}\right]$$

with $D \rightarrow D/(1 \pm A_2)$. $\qquad (28)$

On separating the time interval $(2n-1)T_1$ into a time uncorrelated sequence of $(2m-1)$ shorter driving cycles T_2 along $V_\pm(x)$ (we assume $m > n$; see Fig. 2), one eventually casts the total ratchet current in the form (12) with

$$j_{av}(A_1, A_2) = (1/2)[\overline{j}_-(A_1) + \overline{j}_+(A_1)], \qquad (29)$$

$$\Delta j(A_1, A_2) = (1/2)[\overline{v}_-(A_1) - \overline{v}_+(A_1)], \qquad (30)$$

where

$$\overline{v}_\pm(A_1) = A_1[\mu_\pm(A_1) + \mu_\pm(-A_1)]/2. \qquad (31)$$

We recall that in our notation $\mu_\pm(A)$ is the static nonlinear mobility of the tilted potentials $V_\pm(x) - Ax$.

It is easy to deduce that $|\Delta j(A_1, A_2)|$ may grow larger than $|j_{av}(A_1, A_2)|$ and, therefore, a current reversal may take place for appropriate values of the model parameters, as shown by the simulation results in Fig. 12(a). In fact, already a relatively small modulation of the ratchet potential amplitude at low temperatures can reverse the polarity of the simply rocked ratchet $V_0(x)$. Let us consider the simplest possible case, $\Omega_1 = \Omega_2$ and $\phi_1 = \phi_2$: As the ac drive points in the "easy" direction of $V_0(x)$, namely, to the right, the barrier height $V(x,t)$ is set at its maximum value $\Delta V_0(1 + A_2)$; at low temperatures the Brownian particle cannot overcome this barrier height within a half ac drive period $T_1/2$. In the subsequent half period the driving signal $A_1(t)$ changes sign, thus pointing against the steeper side of the $V(x,t)$ wells, while the barrier height drops to its minimum value $\Delta V_0(1 - A_2)$: Depending on the value of $\Delta V_0/D$, the particle may have a better chance to escape a potential well to the left than to the right, thus making a current reversal possible. Of course, the net current may be controlled via the modulation parameters A_2 and ϕ_2, too.

For both the doubly rocked and rocked-pulsated ratchets, Eq. (12) is symmetric under $m \leftrightarrow n$ exchange. This implies that, as long as the fully adiabatic approximation is tenable, each spectral spike (m,n) of the ratchet current is mirrored by a spike (n,m) of equal strength (see Figs. 3, 4, and 12). This is not true, e.g., in the *partially adiabatic* regime, where the dynamics depends critically on whether Ω_1/Ω_2 or Ω_2/Ω_1 tends to zero.

In the partially adiabatic limit $\Omega_2 \ll \Omega_1$, additional current inversions are observed for the rocked-pulsated ratchet (Fig. 13). In order to understand the mechanism of the negative rectangular current peaks for small driving amplitudes A, let us consider the simplest possible case when $A_2 = 1$, i.e., the potential $V(x,t)$ is switched off completely during the "idle" half of the shorter period [i.e., when $A_2(t) = -A_2$]. Thus, a particle, captured in a potential minimum when $V(x,t)$ is switched on, starts freely moving to the right if $A_1(t) = A_1$ or toward the left if $A_1(t) = -A_1$ when $V(x,t) = 0$. In order to move to the neighboring potential cell, the particle has to travel further than the location of a potential maximum $V_0(x)$ during the "idle" time. Since the left maximum is the closest one, the particle moves on average to the left for low amplitudes. The interval of amplitudes, $A_{start} < A < A_{stop}$ corresponding to the first negative peak can be easily calculated
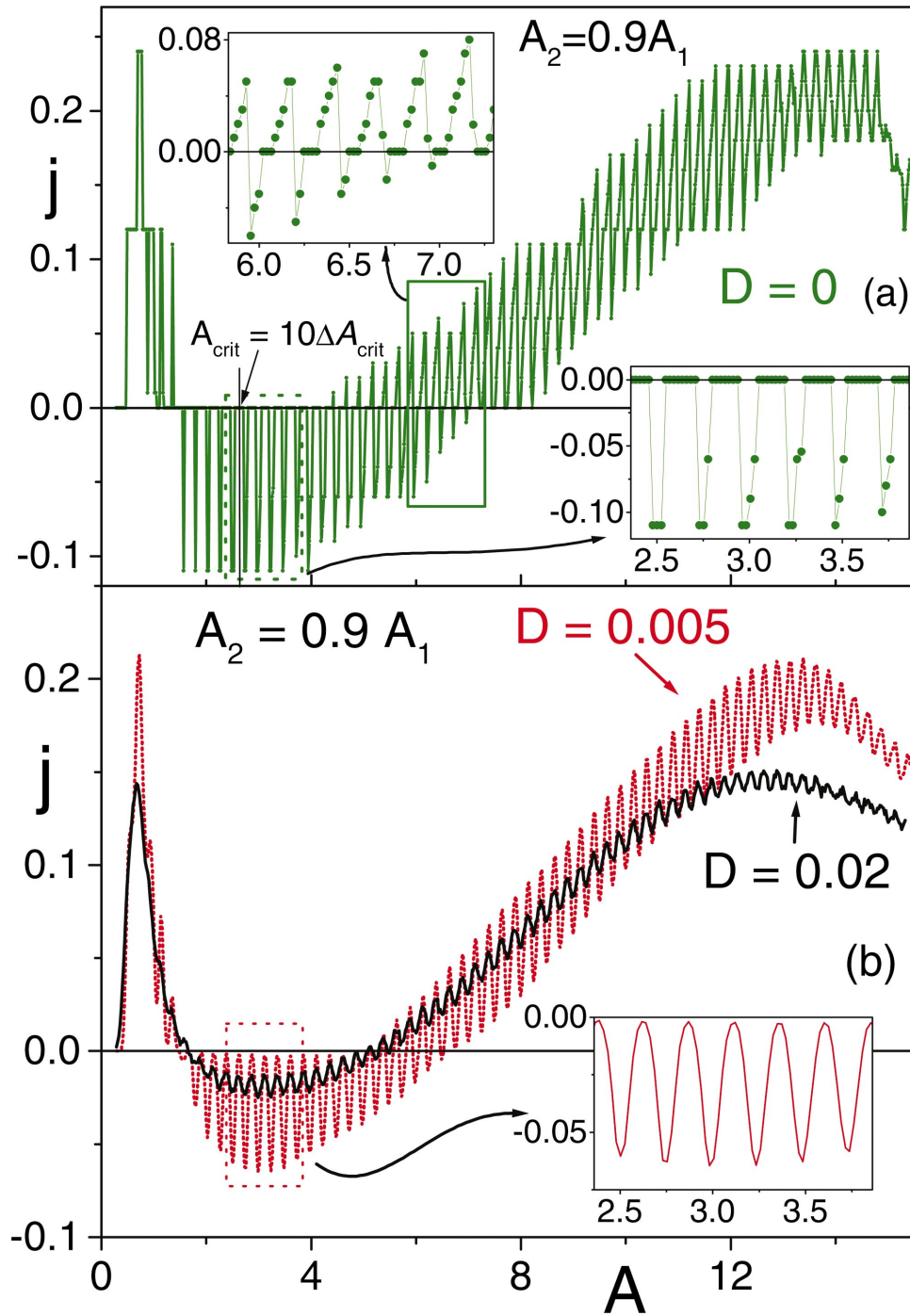
FIG. 8. (Color) Rectified current j versus amplitude A in the doubly rocked ratchet with $A_2=0.9A$, $A_1=A$, $T_1=10^3$, $T_1/T_2=240$. Simulation data for $D=0$ (a), $D=0.005$ (b) (dashed, red curve) and $D=0.02$ (b) (solid, black curve). Potential parameters are as in Fig. 7. Insets: details of the curves for $D=0$ in (a) and $D=0.005$ in (b). See text for the remaining notation.

by imposing the condition that the particle has enough time to reach the location of the left potential maximum during $T_2/2$ but cannot reach the right one spending the same amount of time, i.e., $(T_2/2)A_{start}=l_2$ and $(T_2/2)A_{stop}=l_1$. This equations provide the values $A_{start}=0.36$ and $A_{stop}=0.84$. These values perfectly agree with our simulations (see, Fig. 13). At higher values of A_1 the asymmetry of the potential during the "active" half of the shorter period [i.e., when the potential is switched on: $A_2(t)=A_2$] is responsible for the

rectification. Thus, the current becomes positive in agreement with the polarity of the potential V_+.

B. Mixing of two sinusoidal signals

The effects we discussed above should not be mistaken for a manifestation of harmonic mixing (HM) [21–27], namely, the mechanism where two or more linearly superimposed periodic input signals may develop a phase-dependent
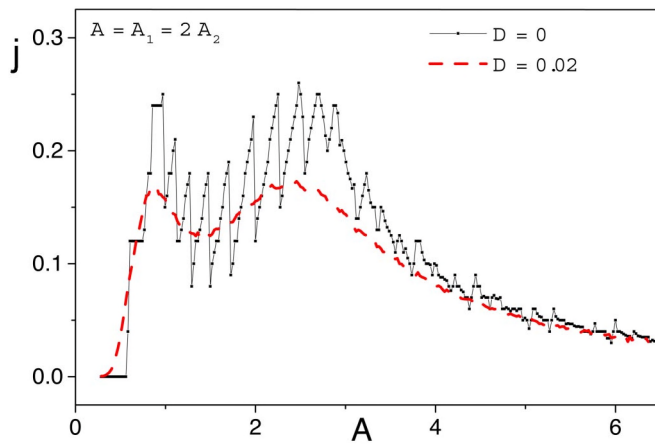
FIG. 9. (Color online) Same as in Fig. 8 but for $A_1=A$ and $A_2=A/2$. Rectangular spikes (at low A) and sawtooth spikes coexist. Noise smooths out the rugged structure at $D=0$; for $D=0.02$ the resulting curve $j(A)$ exhibits two broad peaks.
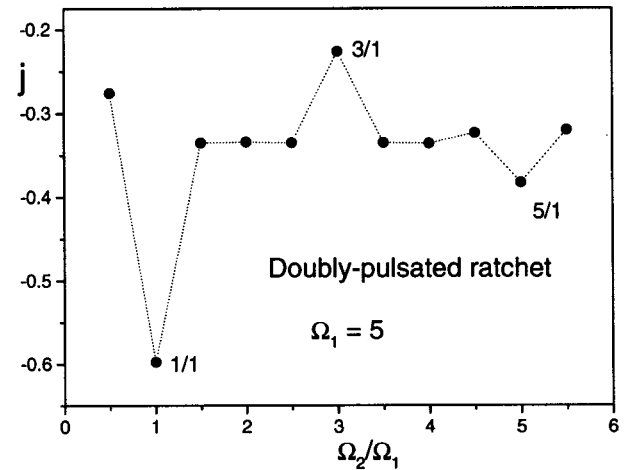

FIG. 11. Rectified current in a doubly pulsated ratchet with piecewise linear potential $V_0(x)$ as in Fig. 1(a) [see Eq. (7)] and driven by two square-wave signals $A_1(t)$, $A_2(t)$ with $\phi_1=\phi_2=\pi$ and $A_1=A_2=0.5$ (simulations). Other parameter values are $q=2$, $l_1=0.9$, $l=1$, and $D=0.6$. Ω_2/Ω_1 for all spikes is indicated explicitly.
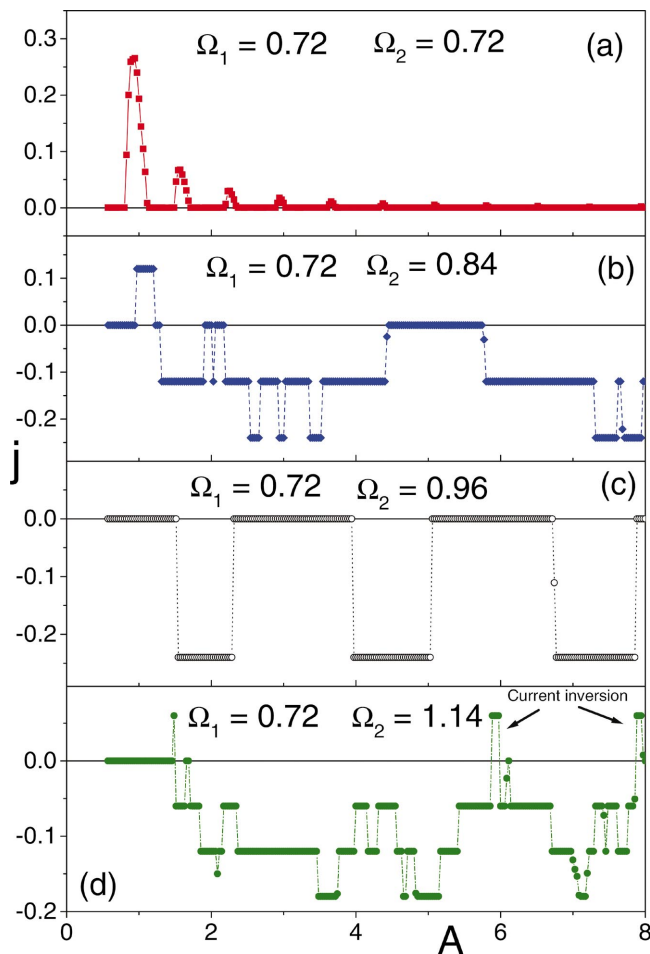

FIG. 10. (Color) Rectified current in the doubly rocked ratchet with $D=0$, $A_1=A_2=A$, and frequencies Ω_1,Ω_2 not subject to the adiabatic condition: (a) $\Omega_1=0.72$, $\Omega_2=0.72$; (b) $\Omega_1=0.72$, $\Omega_2=0.84$; (c) $\Omega_1=0.72$, $\Omega_2=0.96$; (d) $\Omega_1=0.72$, $\Omega_2=1.14$. Potential parameters are as in Fig. 7.

dc output as an effect of nonlinearity. Notice that HM may occur in a symmetric device, too. However, a simple perturbation argument [21] leads one to conclude that in the case of a doubly rocked ratchet HM for a symmetric device in the fully adiabatic regime may be totally suppressed by using *rectangular* wave forms. Moreover, rectification induced by the interplay of additive and multiplicative signals rests upon a sort of *synchronized gating* mechanism peculiar to the case of a rocked-pulsated ratchet and requires no particular substrate symmetry. In this regard, such a mechanism cannot be considered as a HM manifestation, either; rather, it shows some similarities with better studied time-dependent stochastic processes, like stochastic resonance [29], and, more closely related, the control mechanism of stochastic resonance [30]. It thus may explain earlier reports of resonant transport in certain pumped symmetric systems [19]. Note that a binary mixture [31] is a good system for analyzing and clearly separating the signal mixing related to nonlinearity (like HM) and the asymmetry-induced signal mixing; namely, it was shown [31] that nonlinearity and asymmetry result in spikes corresponding to different "winding numbers" of two mixing frequencies.

Asymmetry and nonlinearity-induced mixing are barely separable in the case of *sinusoidal* input signals. This case is analytically less tractable (see Appendix B), and shows significant differences with respect to the square-wave mixing investigated so far. Spikes in the output current spectrum occur for any rational value of $\Omega_2/\Omega_1=m/n$, including *even* fractional harmonics, i.e., $\Omega_2/\Omega_1=2m/(2n-1)$ or $\Omega_2/\Omega_1=(2m-1)/2n$, respectively; but it is no longer symmetric under the exchange of $m\leftrightarrow n$. This is so because the effect of HM cannot be separated from asymmetry-induced mixing. Moreover, these spikes decrease with $m\times n$ much faster than those generated by square-wave input signals, and their sign depends on n,m, in a complicated fashion. However, the mixing effect of two sinusoidal signals is so strong that current reversals may still occur as an effect of frequency com-

mensurability in the case of rocked-pulsated ratchets [see the spikes corresponding to $\Omega_2 = \Omega_1$ and $\Omega_2 = 2\Omega_1$ in Fig. 14(a)]. Moreover, the sign of all the spikes can be easily controlled by changing the phases of the input signals [Fig. 14(b)].

VI. ASYMMETRIC SQUID DRIVEN BY TWO FREQUENCIES

As mentioned before, the reported signal mixing can be realized in a wide variety of physical systems [1,6–11]. Here, we focus on an important example, the asymmetric SQUID [12,13], and demonstrate how the equations describing this type of SQUID can be reduced to our model.

Following Refs. [12,13], we study SQUIDs [Fig. 15(a)] that have two Josephson junctions in one branch of the SQUID loop and one Josephson junction in the other branch. When the junctions are overdamped (i.e., when the resistive term is larger than the capacitive term) and when the SQUID loop has a sufficiently small self-inductance, the dynamical equation describing the evolution of the phase difference φ can be reduced [12] to

$$\frac{\hbar}{eR}\dot{\varphi} = -J_l \sin(\varphi/2) - J_r \sin(\varphi + 2\pi\Phi_{ext}/\Phi_0) + I(t) + \eta(t).$$
(32)

Here, e is the electron charge, R is the junction resistance (we assume the same resistance for all junctions), J_l is the critical current of the junctions on the left branch of the SQUID, while J_r is the critical current of the right junction. This SQUID can be driven by an oscillating external magnetic field [which changes the flux Φ_{ext} in the loop and thus produces the "flashing" potential; Fig. 15(c)] or by an external current $I(t)$, producing a rocking ratchet. To be more precise, we focus here on the case when the SQUID is driven by a current having two frequencies

$$I(t) = I_1 \text{sgn}[\cos(2\pi\tilde{\nu}_1 t - \phi_1)] + I_2 \text{sgn}[\cos(2\pi\tilde{\nu}_2 t - \phi_2)].$$
(33)

Next, we map the dynamics of the SQUID to a "particle" motion by introducing new variables and effective parameters: the particle coordinate $x \equiv (\phi + \pi)/2$, the dimensionless time $\tau \equiv (eRJ_l/2\hbar)t$, the critical current ratio $s \equiv J_r/J_l$, the driving amplitudes $A_{1,2} \equiv I_{1,2}/J_l$, the dimensionless frequencies $\nu_{1,2} \equiv 2\hbar\tilde{\nu}_{1,2}/eRJ_l$, the effective diffusion constant $D \equiv 2ek_BT/\hbar J_l$, the dimensionless flux $\phi_{ext} \equiv 2\pi\Phi_{ext}/\Phi_0$, and the noise ξ obeying the relations $\langle\xi(\tau)\rangle = 0$ and $\langle\xi(\tau)\xi(0)\rangle = 2D\delta(\tau)$. The dynamics of this imaginary particle is described by Eq. (2) for a particular choice of the substrate potential and driving:

$$\dot{x} = \frac{\partial x}{\partial \tau}$$

$$= -\frac{\partial U_{SQUID}}{\partial x} + A_1 \text{sgn}[\cos(2\pi\nu_1\tau - \phi_1)]$$

$$+ A_2 \text{sgn}[\cos(2\pi\nu_2\tau - \phi_2)] + \xi(\tau)$$
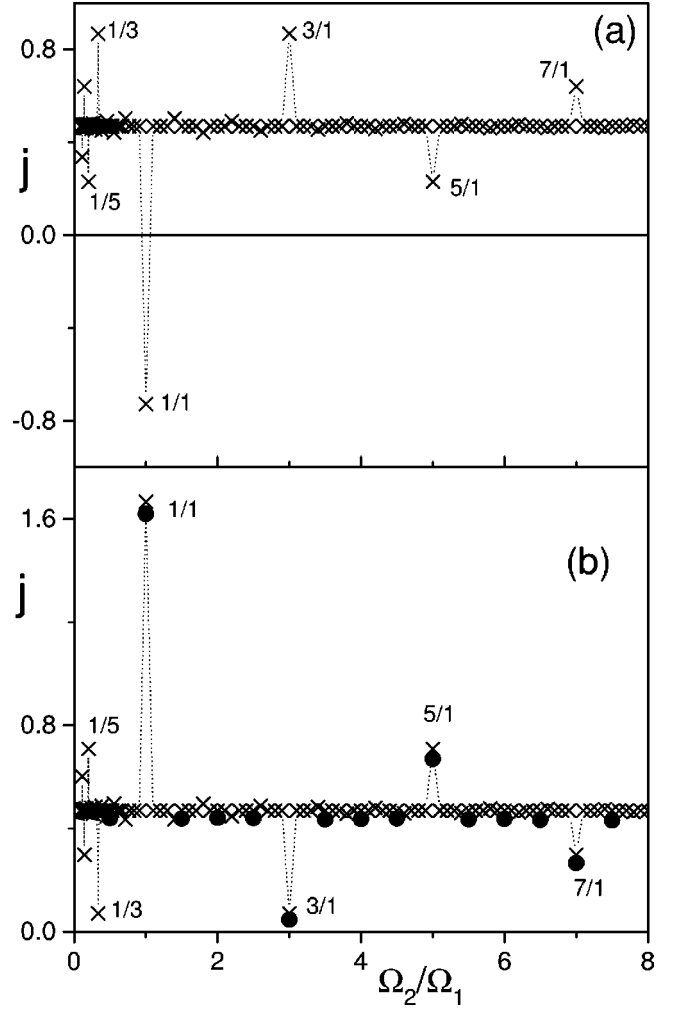(34)

with substrate potential

FIG. 12. Rectified current in a rocked-pulsated ratchet in the fully adiabatic regime. Additive signal $A_1(t)$, with $A_1 = 4$ and $\Omega_1 = 0.01$, and modulating signal $A_2(t)$, with $A_2 = 0.5$; noise level $D = 0.4$. (a) $\phi_1 = \phi_2 = \pi$ (fully adiabatic approximation); (b) numerical simulation (circles) versus fully adiabatic approximation (crosses); $\phi_1 = \pi$ and $\phi_2 = 0$. $V_0(x)$ parameters are $q = 2$, $l_1 = 0.9$, $l = 1$.

$$U_{SQUID}(x) = -[\sin(x) + (s/2)\sin(2x + \phi_{ext} - \pi/2)]. \quad (35)$$

Note that the average velocity is linearly proportional to the dc voltage through the SQUID:

$$\text{(Voltage)} = \frac{J_l R}{2}\langle\dot{x}\rangle \quad (36)$$

and can be directly measured in experiments.

Finally, we show [Fig. 15(b)] that the piecewise linear potential used for simulations approximates well the shape of the SQUID potential U_{SQUID}, at least for certain values of the external field. Moreover, the SQUID dynamics, when changing the magnetic field, can be easily described as a flashing of the potential U_{SQUID}. Thus, the asymmetric SQUID [12,13] is a suitable system to check all predictions made in this work.
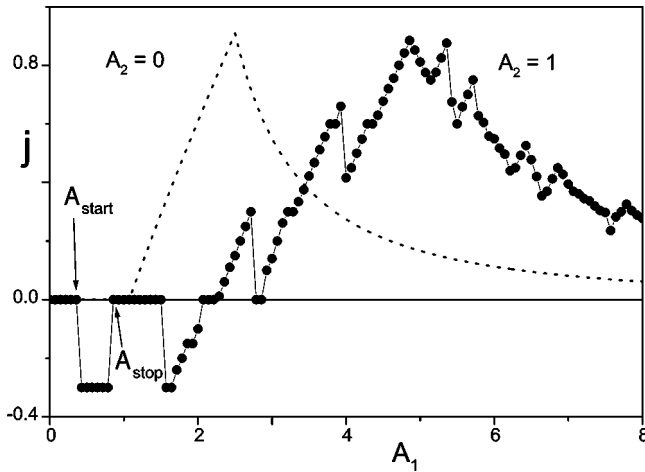
FIG. 13. Rectified current in a rocked-pulsated ratchet: the partially adiabatic regime. Drive parameters are $T_1=10^3$, $T_1/T_2=600$, $\phi_1=\phi_2=0$, $A_2=1$ (black dots) and 0 (dotted curve); $D=0$. $V_0(x)$ parameters are $q=0.75$, $l_1=0.7$, $l=1$.

VII. CONCLUSIONS

In this work we have studied overdamped, directed transport which is controlled via the mixing of two periodic signals through different deterministic and Brownian ratchet setups: the doubly rocked ratchet, the doubly pulsated ratchet, and the rocked-pulsated ratchet. Both analytical and numerical results are presented for the fully and partially adiabatic limits, i.e., when both or at least one of the input frequencies is much lower than the slowest system relaxation rate. The current as a function of the input frequencies exhibits sharp spikes when Ω_2 and Ω_1 are commensurate. This may result in marked current inversions; the interplay of additive and multiplicative signals in a rocked-pulsated ratchet determines a far-reaching rectification mechanism that works also for symmetric substrates (gating mechanism). In the partially adiabatic and in the nonadiabatic regimes, a multiple current inversion phenomenon was found as the driving amplitudes were set to sufficiently close values. Moreover, an unexpected enhancement of the ratchet current was observed for relatively high, but comparable, input frequencies.

The use of nonlinear signal mixing with a second signal in overdamped Brownian motors thus exhibits a rather rich behavior which to some degree already mimics the rich complexity of current reversals as they do occur in driven inertial (underdamped) ratchets [32]. The second time scale introduced by the higher frequency Ω_2 is sufficient to cause a current reversal within the partially adiabatic regime. In contrast to the case with inertia ratchets, the current reversals studied here do not emerge from chaotic dynamics, which is not observed for our overdamped motion, but rather is the result of the nonlinear dynamics induced by the signal mixing.

The results reported here can be employed to control directed transport at mesoscopic and nano scales, for instance in SQUID devices, by engineering the transport characteristics of colloidal mixtures, vortex matter, and other soft-matter systems [1].
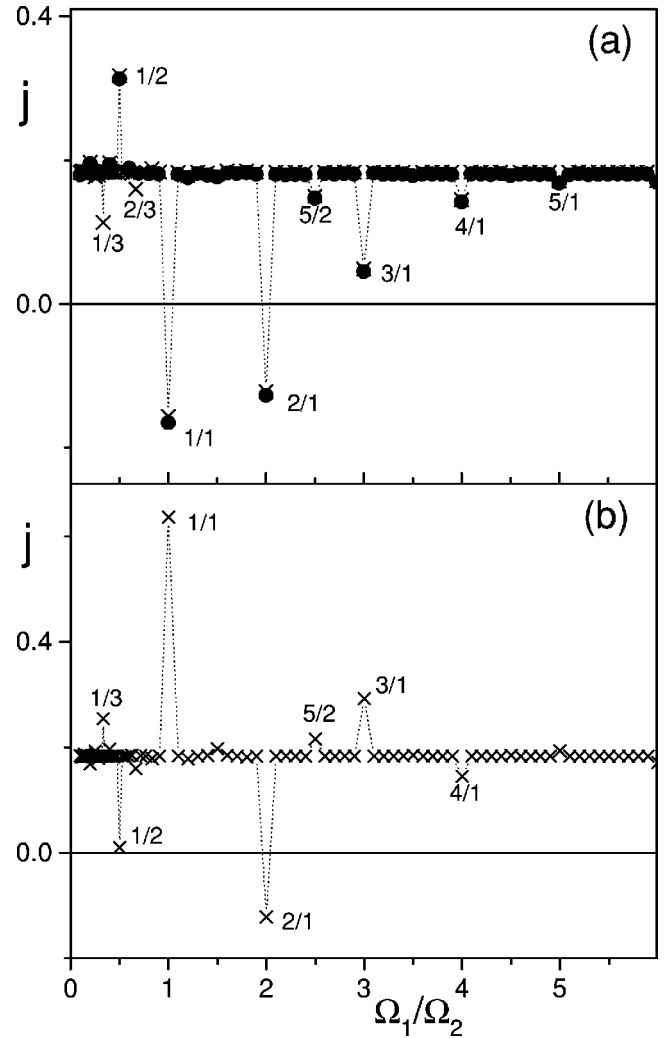

FIG. 14. Mixing of two sinusoidal signals $A_1\cos(\Omega_1 t+\phi_1)$ and $A_2\cos(\Omega_2 t+\phi_2)$ in a rocked-pulsated ratchet. Additive ac drive parameters are $A_1=4$, $\Omega_1=0.01$ with Ω_2 being varied; modulating amplitude $A_2=0.8$; $D=0.2$. (a) Circles, $\phi_1=\phi_2=\pi$, simulation; crosses, $\phi_1=\phi_2=\pi$, adiabatic approximation; (b) $\phi_1=\pi$, $\phi_2=0$, adiabatic approximation. $V_0(x)$ parameters are $q=5$, $l_1=0.9$, $l=1$. Ω_2/Ω_1 of the most prominent spikes is indicated explicitly.

APPENDIX A: AVERAGE PARTICLE CURRENT IN A NOISELESS DOUBLY ROCKED RATCHET (PARTIALLY ADIABATIC LIMIT)

Let us assume that $l_1 > l_2$, $A_1=A_2=A$, $\phi_1=\phi_2$, and $D=0$; moreover, let T_1 be much longer than T_2. First we consider the half (longer) period T_1, when the total driving force is
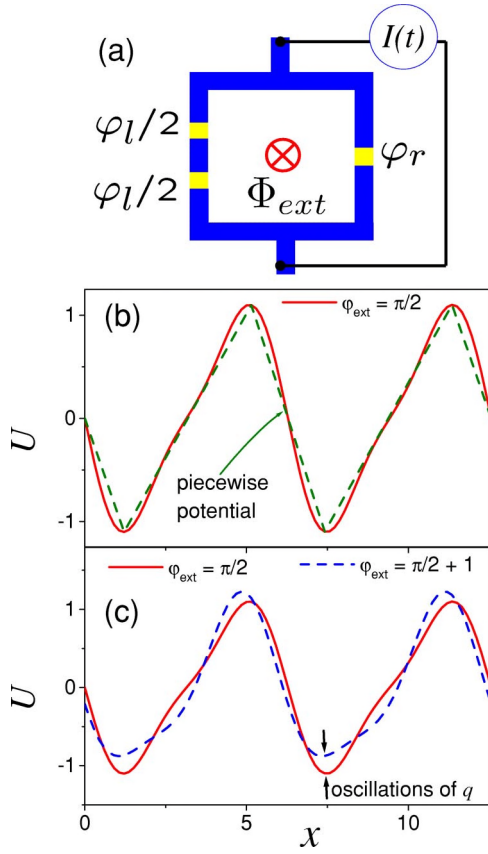
FIG. 15. (Color online) (a) A schematic view of the asymmetric SQUID having two Josephson junctions on the left branch (both of them described by the gauge-invariant phase $\varphi_l \equiv \varphi$) and one josephson junction on the right branch (with phase φ_r). (b) The asymmetric substrate potential [solid (red) curve for $s=0.5$] experienced by a "particle" which mimics the evolution of the phase difference through the asymmetric SQUID. The piecewise linear potential used in previous sections [here shown by the dashed (green) curve] approximates well the real SQUID potential. (c) The flashing SQUID potential is produced by the magnetic field oscillations: the ac field changes from $\phi_{ext}=\pi/2$ [solid (red) curve] to $\phi_{ext}=\pi/2 +1$ [dashed (blue) curve]. The potential heights, denoted by q in Eq. (7), oscillates in time.

either $2A$ or zero. If $A<q/2l_1$, a single particle is confined to a potential minimum (cf. Fig. 16), at any time. If $A>q/2l_1$, the particle drifts toward the right with velocity

$$v_1^+ = 2A - \frac{q}{l_1} \tag{A1}$$

during the half (shorter) period T_2 when the total driving force is equal to $2A$. However, in order to fall into the next potential well, the particle has to overcome a potential barrier height $\Delta V_0 = q$ during a time interval not longer than $T_2/2$. This occurs if the amplitude A exceeds the critical value $A_+^{(1)}$ determined by the condition that the particle reaches the position 1^+ in Fig. 16 during a time interval $t_1^+(A_+^{(1)})$ equal to $T_2/2$, t_1^+ being the time the particle takes to move from a minimum to the closest barrier 1^+, namely,
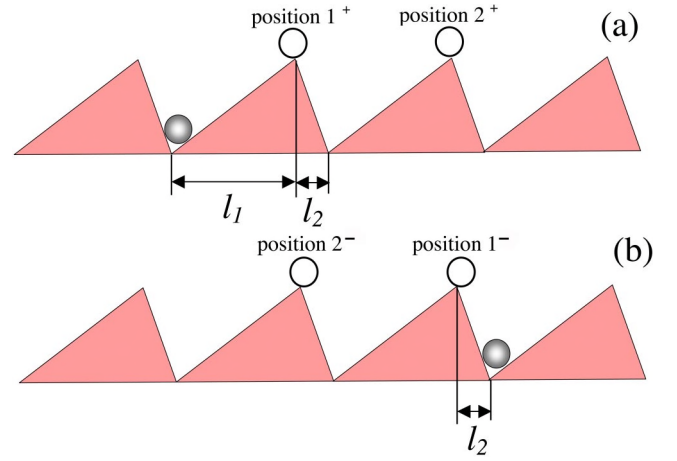

FIG. 16. (Color online) Forward (a) and backward (b) motion of a particle in a periodic asymmetric potential. The notation here is used in Appendix A.

$$t_1^+ = \frac{l_1}{v_1^+} = \frac{l_1}{2A - q/l_1}. \tag{A2}$$

In order to drift past two cells during each short period, the particle should overcome two maxima 1^+ and 2^+ (see Fig. 16) during one half period $T_2/2$. This would take a time $2t_1^+ + t_2^+$ with

$$t_2^+ = \frac{l_2}{v_2^+} = \frac{l_2}{2A + q/l_2} \tag{A3}$$

because the particle has to move twice uphill and once downhill (Fig. 16) with velocities v_1^+ and

$$v_2^+ = 2A + \frac{q}{l_2}, \tag{A4}$$

respectively. Thus, the equation

$$\frac{T_2}{2} = 2t_1^+(A = A_+^{(2)}) + t_2^+(A = A_+^{(2)}) \tag{A5}$$

determines the lowest amplitude $A_+^{(2)}$ for a particle to be displaced by two cells in the shorter modulation cycle T_2. When A is comprised between $A_+^{(1)}$ and $A_+^{(2)}$, a particle has enough time to overcome the first potential barrier, but not the second one. Thus, the particle in Fig. 16 reaches an intermediate location between 1^+ and 2^+ by the time instant when the total driving force A_a drops to zero. During the subsequent time interval when A_a is null, the particle relaxes toward a potential minimum, provided that the frequency Ω_2 is small enough, i.e.,

$$\frac{l_1}{|v_1^+(A=0)|} = \frac{l_1^2}{q} < \frac{T_2}{2} \text{ or } \Omega_2 < \frac{\pi q}{l_1^2}. \tag{A6}$$

Therefore, the average particle velocity v_+ during the half period $T_1/2$ when $A_a(t) \geq 0$ (note that here the average is taken over the shorter cycle T_2) is $v_+(A)=l/T_2$ for $A_+^{(1)}<A<A_+^{(2)}$. By extending the previous argument, we conclude that $v_+(A)=nl/T_2$, with n a positive integer, if in one

half period $T_2/2$ the particle travels a distance longer than $x_+^{(n)} = nl_1 + (n-1)l_2$, but shorter than $x_+^{(n+1)} = (n+1)l_1 + nl_2$. This holds good if $T_2/2$ is longer than $nt_1^+ + (n-1)t_2^+$, but shorter than $(n+1)t_1^+ + nt_2^-$. This corresponds to requiring that $A_+^{(n)} < A < A_+^{(n+1)}$, where $A_+^{(n)}$ is determined by

$$\frac{T_2}{2} = nt_1^+(A_+^{(n)}) + (n-1)t_2^+(A_+^{(n)}). \qquad (A7)$$

The solution to this equation is reported explicitly in Sec. III B. During the following half (longer) period T_1, the driving force $A_a(t)$ is either zero or equal to $-2A$. Thus, an average particle velocity $v_-(A)$ can be obtained from $v_+(A)$ by exchanging $l_1 \leftrightarrow l_2$.

This approach allows us to reproduce both the step structure of the particle current (Fig. 7) driven by one frequency in a tilted potential, and the rectangular tooth structure of the current driven by two signals with equal amplitude A and different frequencies $\Omega_2 \gg \Omega_1$ (Fig. 6).

If $A_2 < A_1$, the qualitative behavior of v_+ for $A_a(t) \geq 0$ (see Fig. 8) remains the same after replacing $2A$ with $A_1 + A_2$, as long as the particle has enough time to relax toward a potential minimum during the time intervals when the total drive is small, i.e., $A_a(t) = \Delta A = A_1 - A_2$. However, this condition may be violated even for $\Omega_2 < \pi q/l_1^2$, since the velocity on the gentle slope over these intervals becomes $v_+(\Delta A) = q/l_1 - \Delta A$. The identity

$$\frac{l_1}{|v_1^+(\Delta A)|} < \frac{T_2}{2}, \qquad (A8)$$

defines the critical amplitude

$$\Delta A_{\text{crit}} = \frac{q}{l_1} - \frac{l_1 \Omega_2}{\pi}, \qquad (A9)$$

so that for $A_1 - A_2 > \Delta A_{\text{crit}}$ the simple velocity quantization nl/T_2 becomes invalid. This means that over the half period $T_1/2$ with $A_a(t) \geq 0$ a driven particle is displaced by n cells plus an additional distance proportional to the drive amplitude. The same argument applies to the average velocity in the half periods $T_1/2$ when $A_a(t) \leq 0$. This explains the changes of the tooth structure of $j(A)$ from "rectangular" to "triangular" on increasing A_1 [see Figs. 8(a) and 9].

APPENDIX B: MIXING OF TWO SINUSOIDAL SIGNALS IN A DOUBLY ROCKED RATCHET (FULLY ADIABATIC LIMIT)

Within the adiabatic approximation, the net current j for any choice of the two signal profiles $|f_1(t)| \leq 1$ and $|f_2(t)| \leq 1$ can be written in the form

$$j = \lim_{t_0 \to \infty} \frac{1}{t_0} \int_0^{t_0} j_{\text{dc}}[Cf_1(t) + Bf_2(t)]dt. \qquad (B1)$$

Here, $j_{\text{dc}} = A\mu(A)$ is the current in a tilted potential $V_0 - Ax$, and C and B are the amplitudes of the mixing signals $A_1(t) \equiv Bf_1(t)$ and $A_2(t) \equiv Cf_2(t)$.

The average above can be rewritten under the "ergodic hypothesis," namely, by replacing the average over time with

the average over the phase space (x,y), the independent variables x and y representing here f_1 and f_2, respectively,

$$j = \int_{-1}^{1} \int_{-1}^{1} dx dy j_{\text{dc}}(Cx + By)P(x)\widetilde{P}(x,y). \qquad (B2)$$

Here, $P(x)$ is the probability (for a random, "uniformly distributed" time t) that $f_1 = x$, while $\widetilde{P}$ is the conditional probability that $f_2 = y$, having set $f_1 = x$. On introducing new variables $z = Cx + By$ and $x' = x$, the integral (B2) reads

$$j = \frac{1}{B} \int_{-C-B}^{C+B} j_{\text{dc}}(z) dz \int_{-1}^{1} P(x)\widetilde{P}[x, (z-Cx)/B] dx. \qquad (B3)$$

Hereafter, we omit the prime in x' for simplicity; $1/B$ is the Jacobian of the transformation. If the frequencies of two signals are incommensurate, then the probability to find $f_2 = y$ is independent of the probability to find $f_1 = x$: $\widetilde{P}(x,y) = P(y)$. Thus, we derive the "incommensurate" net current

$$j_{\text{incomm}} = \frac{1}{B} \int_{-C-B}^{C+B} j_{\text{dc}}(z) dz \int_{-1}^{1} dx P(x) P[(z-Cx)/B] \qquad (B4)$$

and the commensuration spikes

$$\Delta j = j_{\text{comm}} - j_{\text{incomm}} = \frac{1}{B} \int_{-C-B}^{C+B} j_{\text{dc}}(z) dz \int_{-1}^{1} dx P(x)$$
$$\times \{\widetilde{P}[x, (z-Cx)/B] - P[(z-Cx)/B]\}. \qquad (B5)$$

For the case of rectangular signal profiles and $\phi_1 = \phi_2 = 0$, we obtain

$$P(x) = P_{\text{rect}} = \frac{1}{2}[\delta(x-1) + \delta(x+1)], \qquad (B6)$$

while for the sinusoidal profiles $f_1 = \cos(\Omega_1 t)$ and $f_2 = \cos(\Omega_2 t)$

$$P(x) = P_{\text{cos}} = \frac{1}{\sqrt{1-x^2}}. \qquad (B7)$$

Next we need an expression for the conditional probability $\widetilde{P}$. For square waves and $\Omega_1 = 2\Omega_1$, the probability that $f_2 = y$ if $f_1 = 1$, is $(1/2)[\delta(y-1) + \delta(y+1)]$; since f_2 is equal to 1 and -1 for the same amount of time during the half period when $f_1 = 1$. Thus, we derive

$$\widetilde{P}_{\text{rect}}(\Omega_2 = 2\Omega_1) = \frac{1}{2}[\delta(y-1) + \delta(y+1)]. \qquad (B8)$$

For $\Omega_2 = 3\Omega_1$, the time intervals when $f_2 = 1$ and $f_2 = -1$ are different and depend on the conditional value of f_1. One obtains easily

$$\widetilde{P}_{\text{rect}}(\Omega_2 = 3\Omega_1) = \frac{2}{3}\delta(y-1) + \frac{1}{3}\delta(y+1) \text{ if } x=1 \qquad (B9)$$

and

$$\tilde{P}_{\text{rect}}(\Omega_2 = 3\Omega_1) = \frac{1}{3}\delta(y-1) + \frac{2}{3}\delta(y+1) \text{ if } x = -1.$$

(B10)

The general expressions for $\Omega_2 = (2n+1)\Omega_1$,

$$\tilde{P}_{\text{rect}} = \begin{cases} \dfrac{n+1}{2n+1}\delta(y-1) + \dfrac{n}{2n+1}\delta(y+1) & \text{if } x = 1, \\[2mm] \dfrac{n}{2n+1}\delta(y-1) + \dfrac{n+1}{2n+1}\delta(y+1) & \text{if } x = -1, \end{cases}$$

(B11)

follow suit. For the case of cosine signals, the value of $\cos(n\Omega_1 t)$ is known in terms of $\cos \Omega t = x$; hence

$$\tilde{P}_{\cos}(\Omega_2 = 2\Omega_1) = \delta[y - (2x^2 - 1)]$$

(B12)

and

$$\tilde{P}_{\cos}(\Omega_2 = 3\Omega_1) = \delta[y - (4x^3 - 3x)],$$

(B13)

and in the general case

$$\tilde{P}_{\cos}(\Omega_2 = n\Omega_1) = \delta\left\{ y - 1/2\left[(2x)^n - \frac{n}{1}(2x)^{n-2} + \frac{n}{2}\binom{n-3}{1}\right.\right.$$
$$\left.\left. \times (2x)^{n-4} - \frac{n}{3}\binom{n-4}{2}(2x)^{n-6} + \cdots\right]\right\}.$$

(B14)

One conclusion of our approach is that the current spikes are related to the "commensuration" of the input signal profiles f_1 and f_2. Moreover, harmonic mixing in symmetric substrates [i.e., when $j_{\text{dc}}(z) = -j_{\text{dc}}(-z)$] can be given a simple explanation, too. If we consider, for example, the case Ω_2

$= 2\Omega_1$, we realize immediately that the variable $z = Cx + By = Cx + 2Bx^2 - B$ [here we made use of the identities $y = \cos 2\Omega_1 t = 2\cos^2(\Omega_1 t) - 1 = 2x^2 - 1$] does not fill the entire accessible phase space $[-(C+B), C+B]$. Indeed, if $C > 4B > 0$ then $z(x)$ is a monotonic function with values between $z(-1) = B - C$ and $z(1) = B + C$; hence the asymmetric integration domain in (B2).

We also obtained two more useful analytical expressions:

$$j_{\text{incomm}}^{\cos} = \int_{-C-B}^{C+B} K(C,B,z)j_{\text{dc}}(z)dz,$$

$$K = \frac{1}{4}\int_0^\pi \frac{d\phi}{\sqrt{C^2 - (z + B\cos\phi)^2}},$$

(B15)

and

$$j_{\text{incomm}}^{\text{rect}} = \frac{1}{4}[j_{\text{dc}}(C+B) + j_{\text{dc}}(C-B)$$
$$+ j_{\text{dc}}(-C+B) + j_{\text{dc}}(-C-B)].$$

(B16)

If $C > 4B$, then

$$j_{\text{comm}}^{\Omega_2 = 2\Omega_1} = \int_{B-C}^{B+C} dz\, j_{\text{dc}}(z)\frac{1}{M(z)} \times \frac{2B}{\sqrt{8B^2 + 2CM(z) - 2C^2 - 8Bz}}$$

(B17)

with $M(z) = \sqrt{C^2 + 8B^2 + 8Bz}$ for cosine signals.

Therefore, the approach shown here is applicable to both nonlinearity- and asymmetry-induced signal mixing and may be useful to interpret the more complicated case when the two mixing mechanisms cannot be separated (such as in Fig. 14).

[1] P. Hänggi and R. Bartussek, *Nonlinear Physics of Complex System—Current Status and Future Trends*, Vol. 476 of Lecture Notes in Physics (Springer, Berlin, 1996), p. 294; P. Reimann, Phys. Rep. **361**, 57 (2002); R.D. Astumian, Science **276**, 917 (1997); F. Jülicher, A. Ajdari, and J. Prost, Rev. Mod. Phys. **69**, 1269 (1997); R.D. Astumian and P. Hänggi, Phys. Today **55** (11), 33 (2002); P. Reimann and P. Hänggi, Appl. Phys. A: Mater. Sci. Process. **75**, 169 (2002); H. Linke, *ibid.* **75**, 167 (2002), special issue on Brownian motors.

[2] R. Bartussek, P. Reimann, and P. Hänggi, Phys. Rev. Lett. **76**, 1166 (1996).

[3] R. Bartussek, P. Hänggi, and J.P. Kissner, Europhys. Lett. **28**, 459 (1994).

[4] R.D. Astumian and M. Bier, Phys. Rev. Lett. **72**, 1766 (1994).

[5] E. Neumann and A. Pikovsky, Eur. Phys. J. B **26**, 219 (2002).

[6] J.F. Wambaugh, C. Reichhardt, C.J. Olson, F. Marchesoni, and F. Nori, Phys. Rev. Lett. **83**, 5106 (1999).

[7] C.J. Olson, C. Reichhardt, B. Jankó, and F. Nori, Phys. Rev. Lett. **87**, 177002 (2001).

[8] F. Marchesoni, B.Y. Zhu, and F. Nori, Physica A **325**, 78 (2003).

[9] B.Y. Zhu, F. Marchesoni, and F. Nori, Physica E (Amsterdam)

18, 318 (2003); Phys. Rev. Lett. **92**, 180602 (2004).

[10] B.Y. Zhu, F. Marchesoni, V.V. Moshchalkov, and F. Nori, Phys. Rev. B **68**, 014514 (2003); Physica C **388**, 665 (2003); **404**, 260 (2004).

[11] J.E. Villegas, S. Savel'ev, F. Nori, E.M. Gonzalez, J.V. Anguita, R. García, and J.L. Vicent, Science **302**, 1188 (2003).

[12] I. Zapata, R. Bartussek, F. Sols, and P. Hänggi, Phys. Rev. Lett. **77**, 2292 (1996).

[13] A. Sterck, S. Weiss, and D. Koelle, Appl. Phys. A: Mater. Sci. Process. **75**, 253 (2002); S. Weiss, D. Koelle, J. Müller, R. Gross, and K. Barthel, Europhys. Lett. **51**, 499 (2000).

[14] F. Falo, P.J. Martínez, J.J. Mazo, and S. Cilla, Europhys. Lett. **45**, 700 (1999); J.B. Majer, J. Peguiron, M. Grifoni, M. Tusveld, and J.E. Mooij, Phys. Rev. Lett. **90**, 056802 (2003).

[15] P.T. Korda, M.B. Taylor, and D.G. Grier, Phys. Rev. Lett. **89**, 128301 (2002).

[16] S. Savel'ev, F. Marchesoni, and F. Nori, Phys. Rev. Lett. **91**, 010601 (2003); Phys. Rev. E (to be published).

[17] A. Engel, H.W. Müller, P. Reimann, and A. Jung, Phys. Rev. Lett. **91**, 060602 (2003).

[18] F. Marchesoni, Phys. Rev. Lett. **77**, 2364 (1996); G. Costantini and F. Marchesoni, *ibid.* **87**, 114102 (2001).

[19] L. Morales-Molina, N.R. Quintero, F.G. Mertens, and A. Sánchez, Phys. Rev. Lett. **91**, 234102 (2003); M. Salerno and Y. Zolotaryuk, Phys. Rev. E **65**, 056603 (2002).

[20] M. Switkes, C.M. Marcus, K. Campman, and A.C. Gossard, Science **283**, 1905 (1999).

[21] F. Marchesoni, Phys. Lett. A **119**, 221 (1986).

[22] W. Wonneberger, Solid State Commun. **30**, 511 (1979).

[23] I. Goychuk and P. Hänggi, Europhys. Lett. **43**, 503 (1998).

[24] J. Lehmann, S. Kohler, P. Hänggi, and A. Nitzan, J. Chem. Phys. **118**, 3283 (2003).

[25] J. Luczka, R. Bartussek, and P. Hänggi, Europhys. Lett. **31**, 431 (1995); P. Hänggi, R. Bartussek, P. Talkner, and J. Luczka, *ibid.* **35**, 315 (1996).

[26] R. Guantes and S. Miret-Artés, Phys. Rev. E **67**, 046212 (2003).

[27] M. Barbi and M. Salerno, Phys. Rev. E **63**, 066212 (2001).

[28] S. Savel'ev, F. Marchesoni, P. Hänggi, and F. Nori, Europhys. Lett. **67**, 179 (2004); Eur. Phys. J. B **40**, 403 (2004).

[29] L. Gammaitoni, P. Hänggi, P. Jung, and F. Marchesoni, Rev. Mod. Phys. **70**, 223 (1998).

[30] L. Gammaitoni, M. Löcher, A. Bulsara, P. Hänggi, J. Neff, K. Wiesenfeld, W. Ditto, and M.E. Inchiosa, Phys. Rev. Lett. **82**, 4574 (1999); M. Löcher, M.E. Inchiosa, J. Neff, A. Bulsara, K. Wiesenfeld, L. Gammaitoni, P. Hänggi, and W. Ditto, Phys. Rev. E **62**, 317 (2000).

[31] S. Savel'ev, F. Marchesoni, and F. Nori, Phys. Rev. Lett. **92**, 160602 (2004); S. Savel'ev and F. Nori, Nat. Mater. **1**, 179 (2002).

[32] P. Jung, J.G. Kissner, and P. Hänggi, Phys. Rev. Lett. **76**, 3436 (1996); B. Lindner, L. Schimansky-Geier, P. Reimann, P. Hänggi, and M. Nagaoka, Phys. Rev. E **59**, 1417 (1999); J.L. Mateos, Phys. Rev. Lett. **84**, 258 (2000); M. Borromeo, G. Costantini, and F. Marchesoni, *ibid.* **65**, 041110 (2002); H.A. Larrondo, C.M. Arizmendi, and F. Family, Physica A **320**, 119 (2003).